ISBN: 978-3-95450-231-8 ISSN: 2673-5490 doi: 10.18429/JACoW-IPAC2023-THPL083

COMPARISON BETWEEN RUN 2 SEU MEASUREMENTS AND FLUKA SIMULATIONS IN THE CERN LHC TUNNEL AND SHIELDED ALCOVES AROUND IP1/5

D. Prelipcean, G. Lerner, R. García Alía, M. Sabaté Gilarte, F. Cerutti, A. Zimmaro, S. Danzeca
CERN, Geneva, Switzerland

Abstract

The radiation levels in the LHC tunnel and adjacent shielded alcoves on the right side of the Interaction Point 1 (ATLAS detector) and 5 (CMS detector) of LHC at CERN are simulated using the FLUKA Monte Carlo code and compared against Single Event Effect measurements performed with the Radiation Monitor system for Run 2 operation. Considering the complexity and the scale of the simulations as well as the variety of the LHC operational parameters, we find a generally good agreement between measured and simulated radiation levels, typically within a factor of 2 or better.

INTRODUCTION

The scope of this paper is to present a systematic comparison between the simulated and the data measured by radiation monitors used for Radiation to Electronics (R2E) [1, 2] applications at the Large Hadron Collider (LHC) at CERN [3]. For this purpose, Single Event Upset (SEU) measurements performed with the Radiation Monitor (RadMon) system [4] are compared against High Energy Hadron fluence equivalent (HEHeq) values simulated using the FLUKA Monte Carlo code (version 4.1.1, CERN distributed) [5–7].

This is the first study that presents a comparison of HEHeq levels, while previous studies [8] focused on the Total Ionizing Dose (TID) radiation levels. Nevertheless, the measured HEHeq fluences have been previously reported [9] and related mitigation strategies for the electronic systems discussed [10]. More specifically, the benchmark study in this paper has been performed for the tunnel on the right side of the high luminosity Interaction Points 5 (IP5)-CMS detector, but also for the shielded alcoves for IP1-ATLAS detector. The accelerator tunnel is divided into cells [3], and the analysis here covered the Long Straight Section (LSS - up to cell 7) and Dispersion Supressor (DS - up to cell 11) and the beginning of the Arc sector (up to cell 13).

LUMINOSITY-DRIVEN RADIATION LEVELS

The main source of radiation in the LHC tunnel and adjacent shielded alcoves at the high luminosity IPs are inelastic proton-proton collisions in the center of the experiments ($z = 0$ m), whose debris partially propagates in the tunnel leading to radiation showers. As anticipated, the discussion in this paper is focused on the HEHeq fluence (HEHeq), relevant for Single Event Effects (SEE), e.g., SEUs, on machine equipment electronics leading to failures in the operation and accelerator downtime.

Due to the origin of the showers, the radiation levels measurements are assumed (as confirmed in Ref. [11]) to scale with luminosity, which is a measure of the number of inelastic collisions taking place in the IP. The simulations employed in this study are able to (statically) replicate a given LHC configuration, hence the need to identify time periods with constant LHC settings as described in Refs. [8, 11].

THE RadMon DETECTOR

In total, roughly 400 RadMons [4] are placed in strategic locations around the LHC tunnel and its adjacent shielded areas to monitor the radiation field relevant to radiation induced failures in LHC electronics [12]. The RadMon detectors provide measured data on the Total Ionizing Dose (TID) by means of RadFETs (see benchmark example in Ref. [13]), Displacement Damage (DD) by the means of p-i-n diodes, and HEHeq (for particle energies above 20 MeV and intermediate energy neutrons) and Thermal Neutron (THN) fluences by counting SEUs of Static Random-Access Memory (SRAM) memories.

The HEHeq term is employed in the R2E context to designate hadrons carrying enough energy to induce SEUs, usually of the order of MeVs, through indirect ionisation. In general, charged hadrons under 20 MeV are considered not capable to generate SEEs, either due to their very low energy deposition or because they can not simply go through the component package. The 20 MeV limit does not have a universal physical mechanism, but it depends on the device, with recent studies [14] even pointing to a 1.5-3 MeV acute sensitivity for modern electronics. Nevertheless, neutrons can still induce SEEs even at lower energies, as typically modelled via an energy dependent Weibull distribution for intermediate energy neutrons (0.2-20 MeV) and a function decreasing as $E^{-1/2}$ for thermal neutrons, as expected for processes dominated by neutron capture. Taking into consideration both these effects, the total number of SEUs is then defined as the product of fluence (Φ, in units of cm^{-2}) and cross section (σ, in units of cm^2), as:

$$N_{SEU} = \Phi_{THN} \cdot \sigma_{THN} + \Phi_{HEHeq} \cdot \sigma_{HEHeq} \qquad (1)$$

Using precalibrated SRAM detectors with known cross sections, the RadMon can thus be employed to measure HEHeq and thermal neutron fluences. Moreover, one can additionally define a dimensionless quantity called the risk factor (R-factor) that expresses the ratio of fluences of thermal neutrons to high energy hadrons as:

ISBN: 978-3-95450-231-8 ISSN: 2673-5490 doi: 10.18429/JACoW-IPAC2023-THPL083

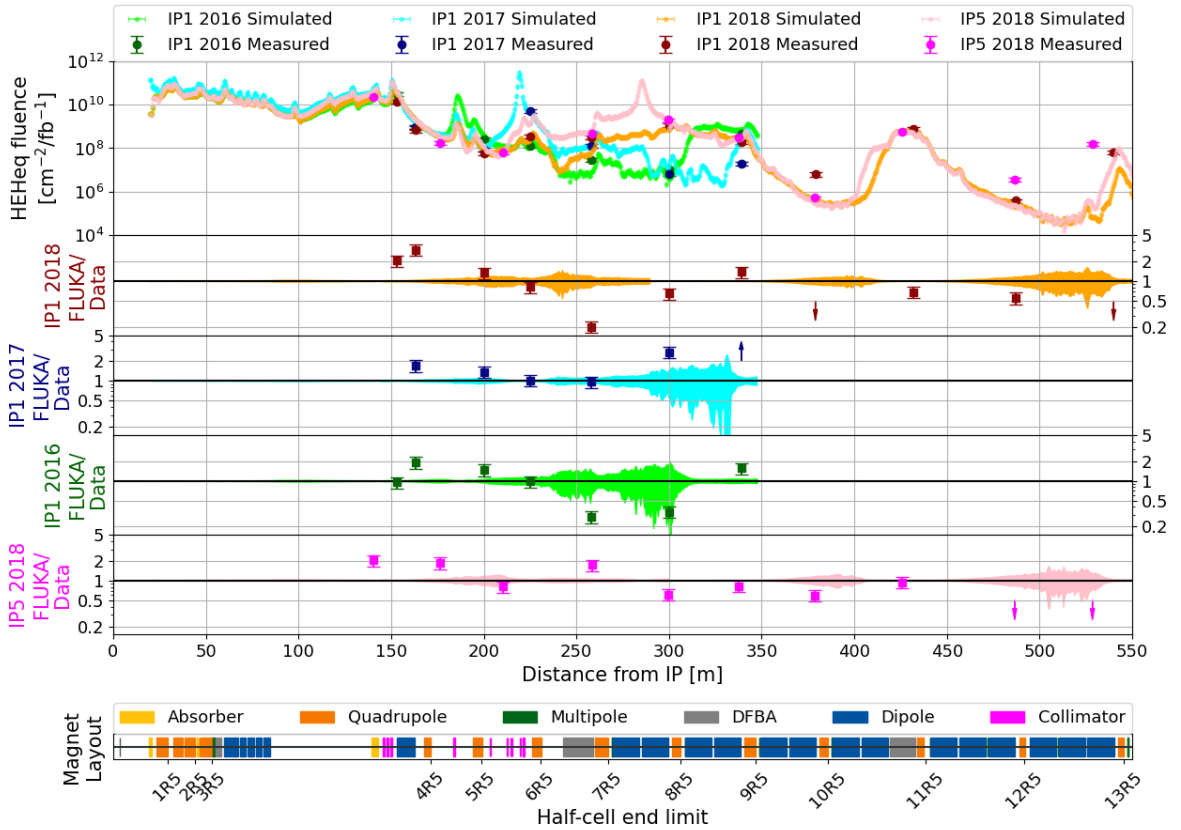

Figure 1: Top panel: Comparison between RadMon data and FLUKA predictions for the tunnel in the right side of the high luminosity IPs for 3 years of Run 2 operation with different configurations: for IP1 (ATLAS detector), 2018 with LSS+DS+ARC TCL456: 15s-35s-park RP: IN (red), 2017 with LSS+DS TCL456: 15s-35s-20s RP: IN (blue), and 2016 with LSS+DS TCL456: 15s-15s-open RP: OUT (green), and for IP5 (CMS detector): LSS+DS+ARC TCL456: 15s-35s-park RP: IN (magenta). Center panels: The ratio of FLUKA simulated values to the RadMon measurements, with arrows indicating outliers outside the plotting range. Lower pad: Machine beamline layout, with markers at the cell limits right of IP.

$$R = \frac{\Phi_{THN}}{\Phi_{HEHeq}} \tag{2}$$

in order to invert equation 1 and compute the fluences from the total number of SEUs. Typical R-factor values are 1.5 for the LHC tunnel, 5 for the RR shielded alcoves and 10 for the UJ and UL alcoves.

Within the large LHC FLUKA geometry, the RadMons are not explicitly modelled (unlike the case of the BLMs in Ref. [8]) due to the minuscule size of the active volume, but the HEHeq fluence is simulated in larger "equivalent" voxels of 20x20x20 cm^3 in the positions of interest. This choice is motivated as well by the fact that, unlike the TID, the hadron fluences are expected to be independent on the material and detector geometry.

HEHeq FLUENCE RESULTS

RadMons in the Accelerator Tunnels

The benchmark between simulated and measured data for the RadMons located in the accelerator tunnels are shown in Fig. 1. The weighted (on the measured fluences) ratios and the standard deviation of FLUKA to measured data for each year are: 0.99 ± 0.58 (2016), 1.13 ± 0.65 (2017) and 1.87 ± 0.88 (2018) for IP1 and 1.87 ± 0.71 (2018) for IP5. Considering the complex accelerator environment and the heterogenity of the radiation field, the observed agreement of the results shown in Fig. 1 is considered to be generally good: the FLUKA predictions reproduce well the measured data trend and the agreement is within a factor of 2 for most RadMons. The local outliers can generate further work in order to understand the origin of discrepancies, for which the possible sources are discussed in the following section.

There are several general considerations to be made about the results in Figure 1, regardless of the LHC configuration, out of which the most important is the global good agreement within a factor of 2 between data and FLUKA simulations. In general, the obvious outliers are considered to arise due to inaccurate simulation geometry modelling. The largest HEHeq levels are usually recorded next to the TAN absorber [15], as it absorbs the flux of forward high energy neutral particles (predominantly neutrons) that are produced at the collision points, generating plenty of secondary showers, and to highlight, also fast neutrons via spallation and evaporation which then scatter and reach thermal energies.

The comparison between the different years of operation reflects the impact of the LHC machine parameters on the

ISBN: 978-3-95450-231-8 ISSN: 2673-5490 doi: 10.18429/JACoW-IPAC2023-THPL083

radiation levels in a local region downstream, if not globally. Three years of Run 2 (2015-2018) with different configurations are shown in Fig. 1. The results are virtually identical up to Cell 5, where the TCL6 closed aperture leads to higher radiation levels between half-cell 7 and half-cell 8 (e.g. with impact on the Quench Protection System [13]). Regionally, there are some systematic trends that can be observed: the RadMons in the ARC region are undersimulated by a factor of 2, eluding to the fact that the collision debris from the IP is no longer the dominant source of radiation (confirming the TID results from Ref. [11]), but the beam-residual gas interaction becomes more important (for a detailed analysis of the measured BLM signals in the ARC, see [16]).

RadMons in the Shielded Alcoves

The benchmark between simulated and measured data for the RadMons located in the shielded alcoves are shown in Table 1. The weighted (on the measured fluences) ratios and the standard deviation of FLUKA to measured data for each year are: 1.31 ± 0.54 (2016), 1.38 ± 0.66 (2017) and 1.46 ± 0.59 (2018), pointing to an oversimulation of the radiation levels. This is considered to be rather good, in order to be on the more cautious side when predicting radiation levels and implementing mitigation measures.

UNCERTAINTIES AND LIMITATIONS

Considering the complexity of the IP1/5 LHC layout, the observed level of agreement between measured data and simulations can be regarded as highly satisfactory. The main sources of uncertainty is considered to be the geometry mismodelling, precision misalingments, etc. It is generally considered that for the complex and large accelerator scenario, the elements are modelled correctly within a 10 cm accuracy and only the radiation monitors may have up to a 1 m shift [18]. Locally, some radiation monitors are placed in the close proximity of strong gradients of radiation, implying that even a slightly shifted position could significantly change the overall agreement. On the detector side, there could be some SEU sensitivity spread amongst the devices, as well as a deviation of the real SEU response from the ideal Weibull model saturating at 20 MeV.

CONCLUSIONS

The main results of this study was to validate the use of simulation tools like FLUKA and their predicting power in the difficult scenario of the LHC accelerator. The general level of agreement that results from this study is a factor of 2 or better, with local outliers. These benchmarking results are of paramount importance to test the consistency between the two independent tools used for assessing the radiation levels in the LHC accelerator environment: (i) radiation monitors, and (ii) FLUKA simulations.

The estimated annual HEHeq levels below the beamline (where electronics racks are often located) varies due to the accelerator operation (e.g. collimator apertures), but it is in the range of $[10^{11}, 10^{13}]$ cm^{-2} up to 150 m, and with local minima down to 10^{8} cm^{-2} up to 350 m, assuming a total of 80 fb^{-1} delivered LHC luminosity per year. Such

Table 1: Comparison of FLUKA and measured data for RadMon SEU response in the IP1 shielded alcoves. The 50% systematic experimental errors considered in this analysis are derived from a similar benchmark study in the more controlled CHARM facility [17], while the statistics one is given from the Poisson counting process as $1/\sqrt{N}$.

Year	RadMon name	Φ_{meas} [cm^{-2}/fb^{-1}]	$\Delta\Phi_{meas}$ (Stat.) [%]	Φ_{sim} [cm^{-2}/fb^{-1}]	$\Delta\Phi_{sim}$ [%]	Φ_{sim}/Φ_{meas} Ratio	$\Delta\Phi_{tot}$ [%]
2016	**SIMA.UJ16.1RM01S**	$4.53{\cdot}10^{6}$	15	$4.46{\cdot}10^{6}$	33	**0.98**	68
	SIMA.UJ16.1RM02S	$8.96{\cdot}10^{7}$	3.3	$1.48{\cdot}10^{8}$	5	**1.65**	50
	SIMA.UJ17.1RM03S	$6.80{\cdot}10^{9}$	0.38	$8.91{\cdot}10^{9}$	1	**1.31**	50
	SIMA.RR17.1RM11S	$1.47{\cdot}10^{7}$	8.3	$2.99{\cdot}10^{7}$	22	**2.03**	59
	SIMA.RR17.1RM12S	$4.84{\cdot}10^{6}$	15	$2.73{\cdot}10^{6}$	53	**0.56**	84
	SIMA.RR17.1RM13S	$2.92{\cdot}10^{6}$	18	$2.39{\cdot}10^{6}$	59	**0.82**	118
2017	**SIMA.UJ16.1RM01S**	$4.53{\cdot}10^{6}$	15	$4.16{\cdot}10^{6}$	28	**0.92**	83
	SIMA.UJ16.1RM02S	$1.07{\cdot}10^{8}$	3.1	$1.40{\cdot}10^{8}$	4	**1.31**	55
	SIMA.UJ17.1RM03S	$6.42{\cdot}10^{9}$	0.39	$8.86{\cdot}10^{9}$	1	**1.38**	50
	SIMA.RR17.1RM11S	$9.84{\cdot}10^{7}$	3.2	$1.57{\cdot}10^{8}$	8	**1.60**	51
	SIMA.RR17.1RM12S	$7.93{\cdot}10^{6}$	11	$1.70{\cdot}10^{7}$	19	**2.15**	63
	SIMA.RR17.1RM13S	$6.21{\cdot}10^{6}$	13	$1.71{\cdot}10^{7}$	18	**2.76**	67
2018	**SIMA.UL16.1RM01S**	$1.09{\cdot}10^{5}$	96	$1.73{\cdot}10^{5}$	40	**1.59**	67
	SIMA.UJ16.1RM02S	$3.63{\cdot}10^{6}$	17	$9.38{\cdot}10^{6}$	7	**2.59**	52
	SIMA.RR17.1RM11S	$3.21{\cdot}10^{7}$	5.6	$4.00{\cdot}10^{7}$	15	**1.25**	52
	SIMA.RR17.1RM12S	$2.11{\cdot}10^{6}$	22	$5.18{\cdot}10^{6}$	50	**2.46**	71
	SIMA.RR17.1RM13S	$4.01{\cdot}10^{6}$	16	$6.29{\cdot}10^{6}$	36	**1.57**	62

ISBN: 978-3-95450-231-8 ISSN: 2673-5490 doi: 10.18429/JACoW-IPAC2023-THPL083

levels are the highest present in the LHC tunnels, and placing equipment here requires dedicated analysis to assess the feasibility of the installation, often involving the development and qualification of radiation tolerant systems.

REFERENCES

[1] Radiation to Electronics (R2E) CERN, website. https://r2e.web.cern.ch/

[2] M. Brugger, "R2E and availability," in *Proc. of Workshop on LHC Performance, Chamonix, France*, 2014.

[3] O. Brüning *et al.*, *LHC Design Report*. CERN, 2004. doi:10.5170/CERN-2004-003-V-1

[4] G. Spiezia *et al.*, "A New Radmon Version for the LHC and its Injection Lines," *IEEE Trans. Nucl. Sci.*, vol. 61, no. 6, pp. 3424–3431, 2014. doi:10.1109/TNS.2014.2365046

[5] FLUKA website. https://fluka.cern

[6] F. collaboration, "New Capabilities of the FLUKA Multi-Purpose Code," *Front. Phys.*, vol. 9, 2022. doi:10.3389/fphy.2021.788253

[7] G. Battistoni *et al.*, "Overview of the FLUKA code," *Ann. Nucl. Energy*, vol. 82, pp. 10–18, 2015. doi:10.1016/j.anucene.2014.11.007

[8] D. Prelipcean *et al.*, "Comparison Between Run 2 TID Measurements and FLUKA Simulations in the CERN LHC Tunnel of the Atlas Insertion Region," in *Proc. IPAC'22*, Bangkok, Thailand, 2022, pp. 732–735. doi:10.18429/JACoW-IPAC2022-MOPOMS042

[9] C. Martinella, "High Energy Hadrons Fluence Measurements in the LHC during 2015, 2016 and 2017 Proton Physics Operations," 2018. https://cds.cern.ch/record/2652458

[10] C. Martinella *et al.*, "Radiation levels in the LHC during the 2015 Pb-Pb and 2016 p-Pb run and mitigation strategy for the electronic systems during HL-LHC operation," 2018. https://cds.cern.ch/record/2647363

[11] D. Prelipcean, "Comparison between measured radiation levels and FLUKA simulations at CHARM and in the LHC tunnel of P1-5 within the R2E project in Run 2," Presented 29 Jul 2021, 2021. https://cds.cern.ch/record/2777059

[12] G. Spiezia *et al.*, "The LHC Radiation Monitoring System - RadMon," in *Proc. 10th Int. Conf. Large Scale Appl. Radiat. Hardness Semicond. Detectors*, vol. RD11, 2011. doi:10.22323/1.143.0024

[13] Y. Aguiar *et al.*, "Radiation to Electronics Impact on CERN LHC Operation: Run 2 Overview and HL-LHC Outlook," in *Proc. IPAC'21*, Campinas, SP, Brazil, 2021, pp. 80–83. doi:10.18429/JACoW-IPAC2021-MOPAB013

[14] A. L. Bosser, "Single-Event Effects from Space and Atmospheric Radiation in Memory Components," December 2017. https://tel.archives-ouvertes.fr/tel-01952831

[15] H. Burkhardt and I. Efthymiopoulos, "Chapter 8: Interface with Experiments. Interface with Experiments," *CERN Yellow Report*, pp. 157–160. 2017. https://cds.cern.ch/record/2120714

[16] K. Biłko *et al.*, "Radiation Environment in the LHC Arc Sections During Run 2 and Future HL-LHC Operations," *IEEE Trans. Nucl. Sci.*, vol. 67, no. 7, pp. 1682–1690, 2020. doi:10.1109/TNS.2020.2970168

[17] D. Prelipcean *et al.*, "Benchmark between measured and simulated radiation level data at the Mixed-Field CHARM facility at CERN," *IEEE Trans. Nucl. Sci.*, pp. 1–1, 2022. doi:10.1109/TNS.2022.3169756

[18] A. Lechner *et al.*, "Validation of energy deposition simulations for proton and heavy ion losses in the CERN Large Hadron Collider," *Phys. Rev. Accel. Beams*, vol. 22, p. 071 003, 7 2019. doi:10.1103/PhysRevAccelBeams.22.071003